Clays and Clay Minerals, Vol. 39, No. 5, 519–530, 1991.

CHARACTERIZATION AND GENETIC INTERPRETATION OF CLAYS IN AN ACID BROWN SOIL (DYSTROCHREPT) DEVELOPED IN A GRANITIC SAPROLITE

DOMINIQUE RIGHI AND ALAIN MEUNIER

UA 721, CNRS, Laboratoires de Pédologie et Pétrologie de altérations hydrothermales, Faculté des Sciences
86022 Poitiers Cedex, France

Abstract—X-ray diffraction and chemical analyses were performed on clay fractions separated from an acid brown soil (Dystrochrept) by means of size fractionations using high-gradient magnetic separation techniques. Breakdown of large phyllosilicates preexisting in the saprolite involved physical fragmentation and mineralogical transformations strongly related to chemical weathering.

Compared to the C horizon, the proportion of chlorite and vermiculite decreased strongly in the silt and coarse-clay fractions of the A1 horizon, but was maintained in the finer clay fraction (<1 μm). The distribution of mica in the different fractions was quite the opposite. Micas are the major component of the A1, 1–2 μm fractions, and their proportion progressively decreased with decreasing fraction size. Thus, it is concluded that during fragmentation and/or simple transformation of the larger phyllosilicates, clusters of chlorite, mica/vermiculite, and vermiculite layers were preferentially affected. A concentration of mica layers took place in the coarse clay fractions as chlorite and vermiculite residues were accumulated in the fine clays.

The process involved the loss of Fe and Mg, leaving, or forming, more aluminous dioctahedral minerals. As the transformation processes occurred, dissolution of preexisting minerals led to the precipitation of amorphous and/or crystalline Fe- and Al-oxides, and possibly of phyllosilicates. The new phyllosilicates appear to be montmorillonitic.

The most abundant end products of the weathering processes in either the A1 or the Bw horizons appeared to be quite different. In the A1 horizon they were identified mainly a hydroxyl-Al (Fe) intergrade smectite (montmorillonite), whereas in the Bw horizon the major component was an intergrade vermiculite originating, at least in part, from chlorite.

Key Words—Soil clays, Weathering, Soil vermiculite, Soil smectite, Hydroxy-Al intergrades, Chlorite, Dystrochrept.

INTRODUCTION

As phyllosilicates are common constituents of soil parent materials, clays from soils of the temperate zone are classically thought to originate from these preexisting phyllosilicates through physical fragmentation and simple transformation (Pédro, 1983). A series of intermediate products may form, the size and composition of which may change during the weathering processes.

Easily weatherable, trioctahedral Fe,Mg-phyllosilicates (chlorite, biotite) are expected to be an important source of soil clays, but dioctahedral Al-micas (muscovite) may also be soil clay precursors (Ross *et al.*, 1982). Transformation of micas to expandable 2:1 minerals is well documented (Fanning *et al.*, 1989; Douglas, 1989). The processes involved are release of K, loss of structural Fe, and decrease in layer charge. Weathering of chlorite in acid soils proceeds through a transformation to vermiculite, with a loss of Fe and Mg (Bain, 1977; Ross *et al.*, 1982; Churchman, 1980). The weathering products of chlorite and trioctahedral micas are therefore expected to have a lower Fe content. Hydroxy-interlayered vermiculite and smectite are formed in acid soils by deposition of hydroxy-Al polymeric components within the interlayers of these expandable phyllosilicates (Jackson, 1963).

Soils, even in the temperate zone, should be considered as a potential environment for neoformation of clay minerals. The identification of the clay phases that would be stable in the physico-chemical conditions of these soils would be very informative.

The aim of this paper was to separate the different clay species from natural mixtures and to differentiate the simple transformation products from neoformed clays. One soil was chosen as a typical example of acid soils developed from a granite saprolite. A typical Humiferous Acid Brown Soil (a Dystrochrept; USDA, 1986) was subjected to particle size fractionation followed by high gradient magnetic separation (HGMS).

Particle size fractionation helps to isolate large, inherited mineral grains from their weathering products that are generally of a smaller size. HGMS concentrates minerals on the basis of their Fe content (Russell *et al.*, 1984; Righi and Jadault, 1988) and thus provides a tool to isolate Fe-rich minerals from aluminous ones (Weed and Bowen, 1990). This approach permitted relatively homogeneous fractions of soil clays to be mineralogically and chemically characterized.

Copyright © 1991, The Clay Minerals Society

https://doi.org/10.1346/CCMN.1991.0390507 Published online by Cambridge University Press

Table 1. Characteristics of the soil horizons.

Horizon	Depth cm	pH (H_2O)	CEC[1]	Org. C[2]	CBD Fe_2O_3[2]	Clay[2] (0–2 μm)
A1	0–8	4.6	0.18	56	12.5	128
A2	8–15	4.9	0.12	48	12.4	132
Bw	15–25	5.1	0.10	25	12.0	118
C	>25	5.3	0.08	12	9.0	53

[1] eq/kg, 105°C, dry sample.
[2] g/kg, 105°C, dry sample.

SOIL MATERIALS

Clays were separated from a typical Humiferous Acid Brown Soil (French classification, CPCS, 1967) or Typic Dystrochrept (Soil Taxonomy, USDA, 1986) of the Plateau de Millevaches, Massif Central, France. The region is hilly and covered by heaths and conifers. The elevations range from 750 to 950 m. Slopes are rather steep but summits are rounded. The climate is cool (8°C mean annual temperature) and humid (1500 mm mean annual precipitation).

The rocky substrate is composed almost exclusively of granite covered by a saprolite mantle, 2–10 m thick. The soil in question formed from this saprolite. Although the age of the saprolite is not precisely known, it may be of Tertiary age. As a consequence of periglacial disturbance of the saprolite during the last glacial period, the present soils are thought to be no older than 15,000 years. Therefore, soil formation in this area was considered to be a distinct process from the saprolite formation. Only the mineralogical changes that took place during soil formation are considered here.

The soil, located on a summit landscape position at elevation 880 m, was selected as a good example of those widely distributed in this region. A previous study (Righi and Borot, 1985) on particle size distribution within the various horizons has demonstrated that the parent material was homogeneous and without any lithologic discontinuity. The soil profile was sampled according to four major horizons, including A1 and A2 (the two most superficial organo-mineral horizons), Bw (with a typical soil structure) and C (the upper part of the saprolite). A short description of the soil profile is given below, together with some important analytical data (Table 1).

0–8 cm: A1, very dark greyish-brown (10YR 3/2) sandy loam, strong, very fine granulate structure, friable, many medium and fine roots, bleached sand grains, few granite gravels, diffuse smooth boundary.

8–15 cm: A2, dark yellowish-brown (10YR 3/4) sandy loam, weak, fine granular structure, friable, common fine roots, few granite gravels, clear smooth boundary.

15–25(35) cm: Bw, dark yellowish-brown (10YR 4/4) sandy loam, weak, subangular blocky structure, friable, few medium roots, granite gravels, diffuse wavy boundary.

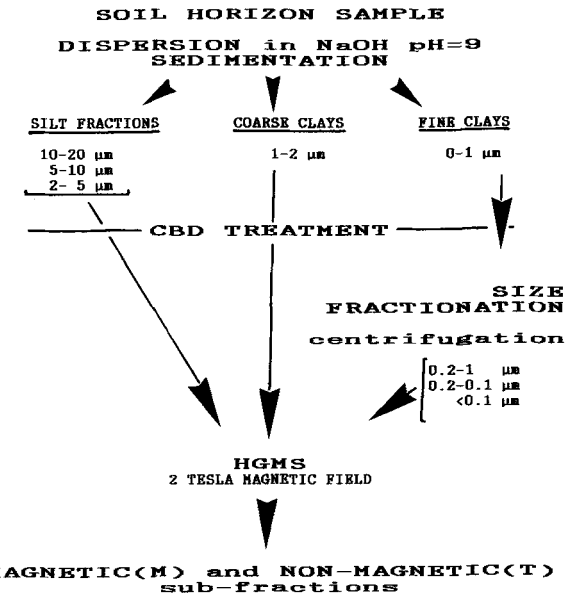

Figure 1. Diagrammatic representation of the successive steps of silt and clay fractionation.

>25(35) cm: C, yellowish-brown (10YR 5/3) sandy loam, weak, subangular blocky structure, friable, gravelly, few roots.

METHODS

The clay and the silt fractions were obtained by sedimentation after treatment of the organic matter with diluted, Na-acetate buffered H_2O_2 (pH = 5) and dispersion in a sodic medium (NaOH) at pH 9. The separated fractions (0–1, 1–2, 2–5, 5–10 and 10–20 μm) were then treated with citrate-bicarbonate-dithionite (CBD) (Mehra and Jackson, 1960) to remove crystalline and amorphous iron oxides and oxyhydroxides. Those iron oxides associated with the phyllosilicate surfaces could affect the magnetic separation. However, CBD treatment may induce a slight alteration of some of the Fe-bearing silicates (Douglas, 1967) and partial dissolution of smectites (Stucki *et al.*, 1984).

The 0–1 μm deferrated clay fraction was further divided into <0.1, 0.1–0.2 and 0.2–1 μm fractions by centrifugation using a Beckman J2-21 centrifuge equipped with the JCF-Z continuous flow rotor.

Each of the clay and silt fractions was then subjected to high gradient magnetic separation (HGMS) according to Righi and Jadault (1988). A magnetic fraction (M), retained on the magnetic filter in a magnetic field of 2 T, and a tail fraction (T) were collected. Figure 1 illustrates the successive steps of the fractionation procedure.

X-ray diffraction (XRD) diagrams were obtained from oriented specimens using a Philips diffractometer and Fe-filtered CoKα radiation. For the silt fractions a classical chart recorder was used. The clay fraction

https://doi.org/10.1346/CCMN.1991.0390507 Published online by Cambridge University Press

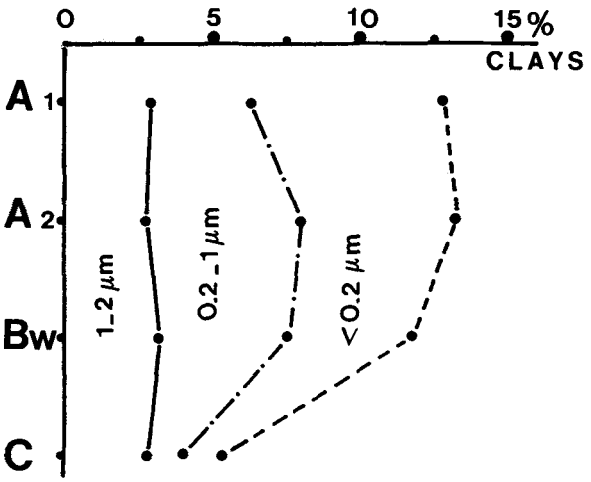

Figure 2. Amounts of the 1–2 µm, 0.2–1 µm and <0.2 µm clay fractions in the different soil horizons, percent of 105°C dry soil. (——): 1–2 µm fraction; (— · —): 0.2–2 µm fraction; (– – –): 0–2 µm (total clay) fraction.

Table 2. Citrate-Bicarbonate-Dithionite extractable Al_2O_3 and Fe_2O_3 from the various fractions (g/kg, 105°C, dry sample).

Sample		Fe_2O_3	Al_2O_3
A1	0–1 µm	70	31
	1–2	39	6
	2–5	23	2
	5–10	12	1
	10–20	8	1
A2	0–1 µm	70	30
	1–2	34	14
	2–5	21	2
	5–10	10	1
	10–20	5	1
Bw	0–1 µm	69	26
	1–2	45	15
	2–5	26	2
	5–10	11	1
	10–20	6	1
C	0–1 µm	20	44
	1–2	13	21
	2–5	6	1
	5–10	7	1
	10–20	5	1

diffractograms were also recorded numerically by a DACO-MP recorder connected to a microcomputer using the Diffrac program of SOCABIM. These diagrams were resolved into their elementary constitutive curves using a least-squares computer program (Lanson and Champion, 1991) that allowed improved measurement of the widths and relative intensities of the diffraction peaks. Pretreatments of the samples included Mg saturation, ethylene glycol solvation, and K saturation followed by heating to 110, 300 and 550°C.

Total analyses were performed on CBD-treated samples according to Jeanroy (1972). Si, Al, Fe, Ti, Mg, Ca, Na and K were analyzed by atomic absorption spectroscopy (AAS).

Cation exchange capacity (CEC) was obtained by saturation with Mg, the excess of Mg salt ($MgCl_2$) being carefully washed with ethanol. Mg was then exchanged by NH_4 and analyzed in the exchange solution by AAS.

An acid dissolution treatment (1 N HCl; 80°C overnight) according to DeConinck *et al.* (1975) was used to dissolve chloritic materials, and possibly other trioctahedral minerals (MacEwan and Wilson, 1980). Dissolved Al, Fe, Mg and K were analyzed by AAS.

CEC and HCl dissolution treatments were also performed on CBD-treated samples.

A M^+-4Si-R^{2+} ternary system (Meunier and Velde, 1989) was used to represent graphically the chemical composition of the silt and the clay fractions. An average structural formula was calculated for each fraction on a $O_{10}(OH)_2$ basis. M^+ was taken as the sum of the nonexchangeable K content plus the number of charges deduced from the measured CEC. Coordinates for reference low- and high-charge montmorillonite and beidellite were taken from Meunier and Velde (1989). Such a system permitted the separation of phyllosilicates according to their layer charge (M^+ pole), the Si content of the tetrahedral sheet (4Si pole), and the divalent cations in the octahedral sheet (Mg^{2+} in the present study).

RESULTS

The amount of clay in the samples and the proportions of the <0.2, 0.2–1 and 1–2 µm fractions are shown in Figure 2. Total clay (0–2 µm) increased from 50 g/kg in the C horizon to 120 g/kg in the A1 horizon. Only the fine fractions (<0.2 and 0.2–1 µm) were increased by soil formation relative to the C horizon.

The CBD-extracted Fe and Al, expressed as Fe_2O_3 and Al_2O_3, are given in Table 2. These amounts decreased with an increase in particle size, but was about the same from one horizon to another. An exception is the C horizon where Fe_2O_3 was lower and Al_2O_3 higher.

Ratios for the magnetic (M) to nonmagnetic (T) fractions are given on a semi-quantitative basis in Table 3. The most important feature is that the M-fractions decreased in the most superficial horizon (A1). In other words, from the C to the A1 horizon, the tendency was to concentrate a more abundant <0.1 µm T-fraction, while the <0.1 µm M-fraction was strongly reduced.

Mineralogy of the silt fractions

M- and T-fractions from the silt samples exhibit clearly different XRD diagrams (Figure 3). In the T-fractions, the most intense reflections are those of mica (0.989, 0.498 and 0.333 nm), quartz (0.424, 0.333 nm), and feldspar (0.321 and 0.319 nm). Only traces of quartz and feldspar were detected in the M-fractions,

https://doi.org/10.1346/CCMN.1991.0390507 Published online by Cambridge University Press

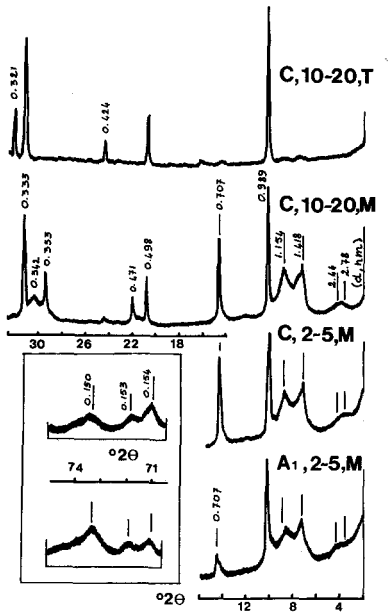

Figure 3. XRD diagrams for silt fractions (Mg saturated) from the C and A1 horizons. CoKα radiation, d-spacings in nm.

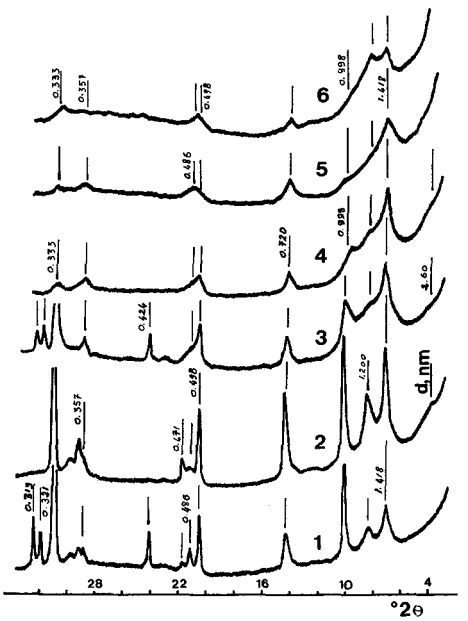

Figure 4. XRD diagrams for Mg-saturated clay fractions. CoKα radiation, d-spacings in nm. 1: C, 1–2 μm T-fraction; 2: C, 1–2 μm M-fraction; 3: A1, 0.2–1 μm T-fraction; 4: A1, 0.1–0.2 μm T-fraction; 5: Bw, <0.1 μm T-fraction; 6: A1, <0.1 μm M-fraction.

but the XRD diagrams exhibit reflections of mica (0.989 and 0.498 nm), chlorite and vermiculite (1.420, 0.707, 0.471 and 0.353 nm), interstratified mica/vermiculite (2.440, 1.154 and 0.342 nm), and probably interstratified chlorite/vermiculite (2.780 and 1.420 nm). According to the peak positions (1.154, 0.342 nm) the interstratified mica/vermiculite contains 70% mica layers (Reynolds, 1980). Within the M-fractions a decrease in the intensity of the 0.707, 0.471 and 0.353 nm reflections is observed for sample from the A1 horizon. This is indicative of a decrease in the amount of chlorite in that fraction. The 2–5 μm M-fractions also exhibited three reflections at 0.150, 0.153 and 0.154 nm that are attributed to the (060) reflections of both trioctahedral (0.153 and 0.154 nm) and dioctahedral minerals. The relative intensity of the 0.150 nm reflection is greater for the A1, 2–5 μm, M-fraction as compared to the same M-fraction from the C horizon.

Mineralogy of the clay fractions

From the C horizon sample only, the 0.2–1 and 1–2 μm fractions were collected in sufficient amounts to allow further study. As in the silt fractions, quartz and feldspars were concentrated in the T-fractions along with smaller amounts of gibbsite (0.486 nm) and kaolinite (0.720 and 0.357 nm) (Figure 4). The other phyllosilicate phases were almost identical and composed of mica (0.998 nm), vermiculite (1.408 nm), and interstratified mica/vermiculite (1.190 nm) (Figure 4). Chlorites (0.471 and 0.353 nm) were also identified, but mainly in the M-fractions.

From the A and Bw horizons a complete series (<0.1, 0.1–0.2, 0.2–1 and 1–2 μm) was obtained. Quartz was not identified in the <0.2 μm fraction, nor even in the nonmagnetic fractions. Small amounts of kaolinite and

Table 3. Relative amounts of magnetic (M) and nonmagnetic (T) fractions in the coarse and fine clays from the soil horizons (semiquantitative estimation).

	Size (μm)							
	1–2		0.2–1		0.2–0.1		<0.1	
	M	T	M	T	M	T	M	T
A1	**	****	**	****	**	****	*	*****
A2	***	***	**	****	**	****	**	****
Bw	***	***	***	***	***	***	**	****
C	***	***	***	***	—	—	—	—

—: no fraction; *: very minor; **: minor; ***: half of the bulk fraction; ****: major; *****: dominant.

https://doi.org/10.1346/CCMN.1991.0390507 Published online by Cambridge University Press

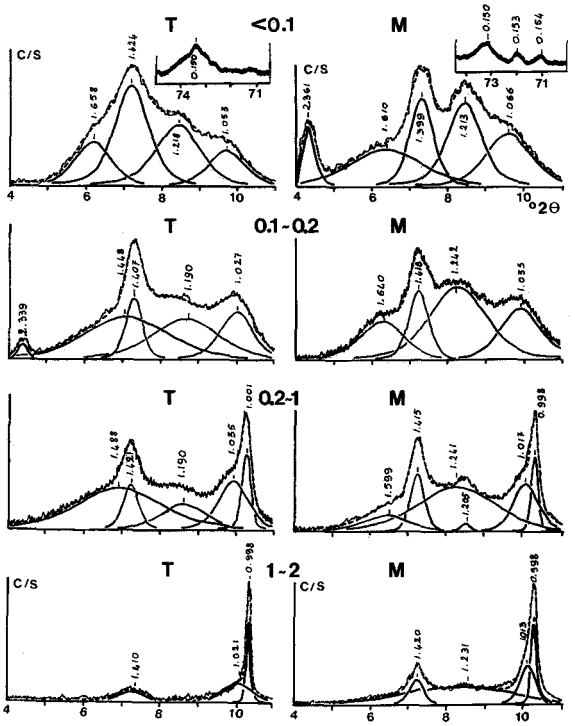

Figure 5. Resolved XRD diagrams for the A1 horizon clay fractions (Mg saturated and ethylene glycol solvated). (——): experimental curve; (——): computed elementary curves; (– – –): best-fit computed curve. CoKα radiation, d-spacings in nm.

gibbsite may be present in the <1 μm fractions (Figure 4).

A complete set of resolved XRD diagrams from the A1 clay fractions is shown in Figure 5. In the range of 4–11° 2θ only two major reflections were obtained from the 1–2 μm fractions. These were attributed to mica and vermiculite. The mica peak was resolved into two curves. One is very sharp, indicative of a well-crystallized mineral. The second is broader and less intense, and thought to represent interstratified expandable layers. Resolution of the 1–2 μm M-fraction gave a supplementary, very broad reflection centered at 1.23 nm that may indicate few mica/vermiculite interstratified layers. It may also represent an increase in the background level caused by amorphous compounds, even though these were supposed to be removed by the CBD treatment.

Compared to that of the coarse clay fraction, the XRD diagrams from the fine fractions (<1 μm) were different. Resolution of these diagrams gave five basic curves. From the 0.2–1 to the <0.1 μm fractions the following changes were observed:

1. A sharp peak at about 1.00 nm, still present in the 0.2–1 μm fractions, disappeared from the finer fractions. Only the second broad curve of the mica peak

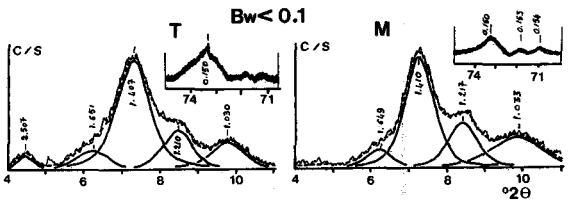

Figure 6. Resolved XRD diagrams for the Bw horizon finest clay fractions. Mg saturated and ethylene glycol solvated, CoKα radiation, d-spacings in nm, curves as in Figure 5.

persisted, but with its position shifted (1.02–1.07 nm) and its width increased (0.7–1.4° 2θ at half height).

2. A peak at about 1.20 nm showed increased intensity and decreased width from the 0.2–1 to the <0.1 μm fractions.

3. A peak at about 1.40 nm became the most intense in the finest fractions. On the 0.2–1 and 0.1–0.2 μm, T-fraction diagrams the 1.40 nm reflection is composed of two basic curves with either a large or a small width. This is indicative of the presence of two types of vermiculite particles, one with few layers in the stacking sequence (large width) and the other with better-ordered stacking.

4. Smectite layers (basic curve with a maximum of intensity at about 1.60 nm) were observed in all the M-fractions, but only in the <0.1 T-fraction. For the M-fractions the peak intensities for smectite layers increased toward the finer fractions. After K saturation, heating to 110°C and glycolation, the smectite layers in the <0.1 μm M-fraction reexpanded, but not in the <0.1 μm T-fraction. The former were identified as low charge layers and the latter as high charge layers.

5. A strong peak at 2.38 nm is present in the <0.1 μm M-diagram indicating an ordered, interstratified mica/vermiculite (first order reflection).

The same general trend was observed for the fractions from the A2 (not shown) and Bw horizons (Figure 6), except for the finest fractions from the Bw horizon. Here the relative intensity of the peak at 1.40 nm was greater than for the equivalent A1 horizon sample indicating less smectite and more vermiculite layers in the Bw sample than in the A1 sample. Moreover, the <0.1 μm M- and T-fractions were identical. All the <0.1 μm T-fractions are composed primarily of dioctahedral minerals as indicated by a broad reflection near 0.150 nm (Figures 5, 6). However, remnants of trioctahedral minerals were identified in the <0.1 μm M-fractions by peaks at 0.153 and 0.154 nm.

Heat treatments. The K-saturated clays were heated to 110, 300 and 550°C. Collapse of the interlayers was always progressive and incomplete for all the samples, even after heating to 550°C. This resulted in an XRD peak asymmetric toward the small 2θ angles (Figure 7).

https://doi.org/10.1346/CCMN.1991.0390507 Published online by Cambridge University Press

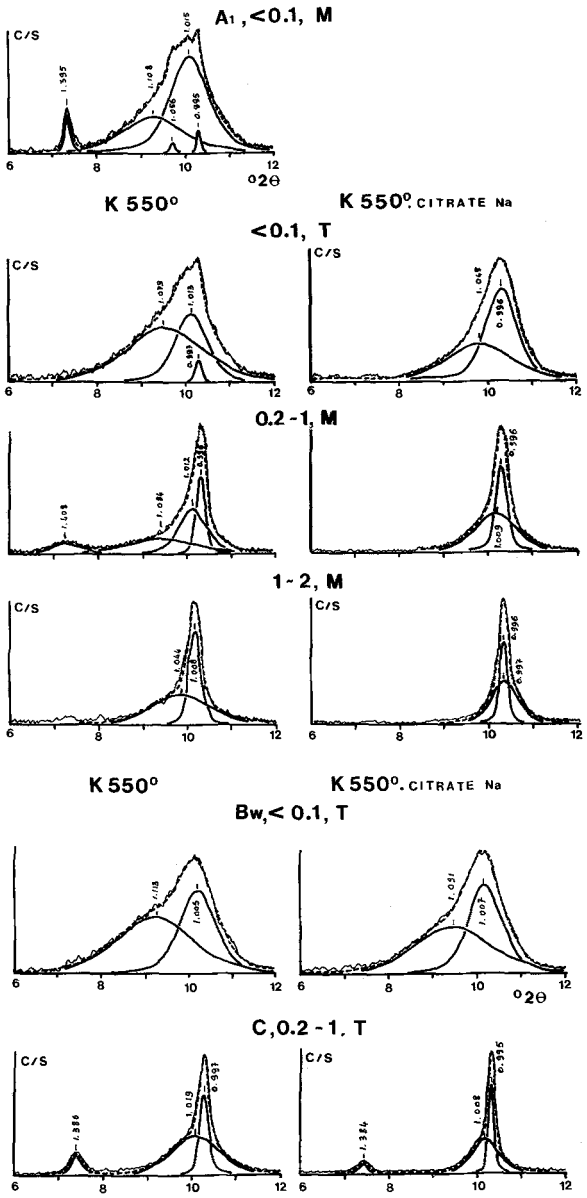

Figure 7. Resolved XRD diagrams from some K-saturated and heated (550°C) fractions, before and after the Na-citrate treatment. CoKα radiation, d-spacings in nm, curves as in Figure 5.

The diagrams were resolved into two or three curves. A sharp curve with an intensity maximum at about 1.00 nm was observed only for the 0.2–1 and 1–2 μm fractions (except A1, <0.1 μm where the intensities were low). This curve is attributed to completely collapsed interlayers. A broad curve with a maximum at about 1.01 nm is associated with the previous curve. Its intensity increased from the coarse to the fine fractions, where it was prominent. Moreover, a second curve centered at slightly higher d-spacings (1.08–1.11 nm) is an important component of the XRD diagrams from the finest fractions. These curves were attributed to interstratification of collapsed and uncollapsed interlayers. A greater proportion of uncollapsed interlayers should produce a larger d-spacing.

Table 4. Composition of Na-citrate extracts.

Sample	Al_2O_3		Fe_2O_3		MgO	
	(1)	(2)	(1)	(2)	(1)	(2)
A1, <0.1 μm T	23.0	8	13.7	18	0.7	4
A1, 0.2–1 μm M	11.0	4	5.6	6	0.7	4
A1, 1–2 μm M	7.0	3	0.9	2	0.6	4
Bw, <0.1 μm T	27.0	9	14.9	22	9.2	37
C, 0.2–1 μm T	24.0	10	3.6	6	2.7	30

(1) g/kg, 105°C, dry sample; (2) percent total oxide.

An additional small peak at about 1.40 nm was observed in the diagrams from the C, 1–2 and 0.2–1 μm and A1, 0.2–1 and <0.1 μm M-fractions, but is not present in the Bw <0.1 μm fractions. It is attributed to chlorite layers.

Na-citrate treatment. A Na-citrate treatment (Tamura, 1958) was performed on some samples in an attempt to extract contaminants preventing the complete collapse of the interlayers. XRD diagrams from the treated samples were compared to those of the corresponding untreated samples (Figure 7).

For the C horizon, 0.2–1 μm T-fraction few changes were observed. The treated sample is characterized by a decrease in the intensity of the 1.40 nm peak, and further collapse of the interlayers following K saturation and heating to 550°C.

For the Bw horizon, <0.1 μm T-fraction a small decrease in the relative intensity of the 1.09 nm peak was observed. The diagram of the K-saturated, 550°C sample remained strongly asymmetrical.

For the A1 horizon samples the efficiency of the treatment varied according to the fraction tested. For the coarse fraction (1–2 μm) the treatment resulted in a complete collapse of the interlayers, as indicated by a symmetrical peak at 0.996 nm. The same result was obtained from the 0.2–1 μm T-fraction. When compared to the untreated sample, the peaks at 1.40 nm and 1.08 nm disappeared from the diagram of the treated sample. For the <0.1 μm T-fraction, an improved collapse was observed, but the diagram was still asymmetrical and resolvable into two basic curves. However, compared to the Bw horizon, <0.1 μm T-fraction, the effect of the Na-citrate treatment was more evident. Moreover, the XRD behavior of the glycolated samples from either the A1 or Bw, <0.1 μm T-fractions was different (Figure 8). Compared to the untreated sample, the proportion of swelling layers (1.65 nm) was strongly increased in the A1, <0.1 μm T-fraction, but such increase was far less important for the Bw, <0.1 μm T-fraction. A Greene-Kelly (1953) test was performed

https://doi.org/10.1346/CCMN.1991.0390507 Published online by Cambridge University Press

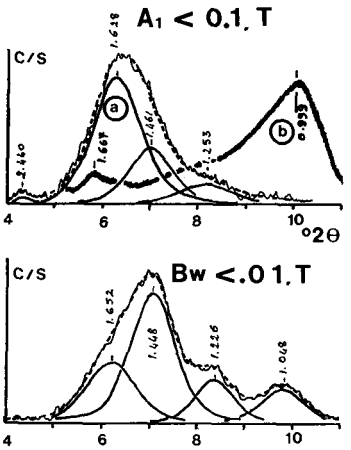

Figure 8. Resolved XRD diagrams from the A1 and Bw horizon, <0.1 μm T-fraction after Na-citrate treatment. A1 horizon sample: a–Mg saturated and ethylene glycol solvated, curves as in Figure 5; b–Li saturated, heated and ethylene glycol solvated (Greene-Kelly test), experimental curve. Bw horizon sample: Mg saturated and ethylene glycol solvated, curves as in Figure 5. CoKα radiation, d-spacings in nm.

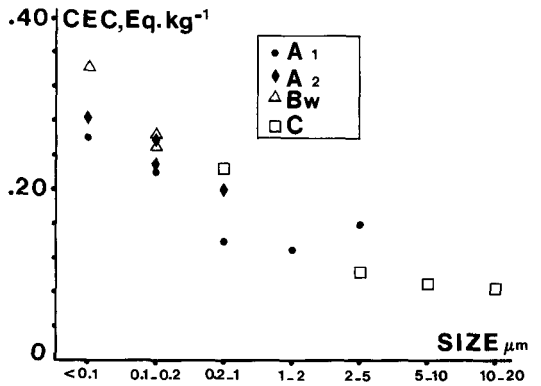

Figure 9. CEC values for the silt and clay fractions.

on the A1, <0.1 μm T-fraction. The result clearly indicated that the smectite layers were essentially montmorillonitic (Figure 8).

The composition of the Na-citrate extract was also different according to the sample from which it was obtained. From the C horizon, 0.2–1 μm, and Bw horizon, <0.1 μm T-fractions, large amounts of MgO (37 and 30% of total MgO, respectively) were extracted with Al_2O_3 and Fe_2O_3 (Table 4). Conversely, only small amounts of MgO were extracted from the A1 fractions. Al_2O_3 and Fe_2O_3 were largely extracted from the A1, <0.1 μm T-sample, and to a lesser extent from A1, 0.2–1 and 1–2 μm M-fractions.

Cation exchange capacity

CEC varied from 0.085 eq/kg (C, 10–20 μm M-fraction) to 0.344 eq/kg (Bw, <0.1 μm T-fraction), and increased from the larger to the finer fractions (Figure 9). Within the fine clay samples (<1 μm) the CEC was the lowest for those from the A1 horizon. The highest CEC was observed in the Bw horizon fine clays (<0.1 μm).

Total chemical analysis

The results from the chemical analyses are given in Table 5, and the relative amounts in Al, Fe and Mg atoms are plotted in a triangular coordinate diagram with the three poles attributed to 100% Al, 50% Fe, and 50% Mg, respectively. Except for the three finest fractions from the A1 horizon, all the representative plots fell onto a line tied to the 100%-Al pole (Figure 10). This indicates that the Fe/Mg atomic ratio is equal for all these samples. Moreover, the relative Al content increases from the silt fractions in the C horizon to the finest clay fractions in the Bw and A2 horizons. The plots for the three finest fractions from the A1 horizon are shifted toward a higher Fe/Mg ratio line.

The Si/Al ratios (Figure 11) fall between 1.6 and 1.8 for the silt and coarse clay fractions (1–2 μm), but are lower (1.2–1.4) for the fine clay fractions. The lowest values (0.8, 0.9 and 1.1) were observed in the finest fractions from the A1 horizon.

The CEC values and the Si/Al ratios (except for those of the A1 horizon) are strongly correlated with the K_2O content. The regressions are: CEC eq/kg = -9.26 K_2O% + 0.56; r = -0.94 (Figure 12) and Si/Al = 0.21 K_2O% + 0.63; r = 0.91 (the A1 horizon fine fractions are excluded) (Figure 13).

HCl dissolution

1 N HCl dissolution treatment was done on the <0.1 μm T-fractions from the Bw and A1 horizons. Fe_2O_3 was completely extracted from the two samples, but only 59% of the total Al_2O_3 was removed (Table 6). The contents of K_2O and MgO extracted by the treatment were strongly different according to the sample. 92% of MgO and 90% of K_2O were extracted from the Bw horizon sample, but only 47% and 49%, respectively, from the A1 horizon.

DISCUSSION

The silt and clay fractions from the C horizon contain chlorite layers that could not be separated by HGMS from the mica, vermiculite, and interstratified mica/vermiculite layers. This suggests that all these layers were closely associated in the same silt or clay particles. If ferruginous chlorite layers had been present as discrete particles, they should have been easily separated by HGMS (Ghabru *et al.*, 1990; Weed and Bowen, 1990; Righi and Jadault, 1988).

Compared to that of the C horizon, the proportion of chlorite layers is strongly reduced in the fine silt fraction (2–5 μm) of the A1 horizon. Moreover, chlorite

https://doi.org/10.1346/CCMN.1991.0390507 Published online by Cambridge University Press

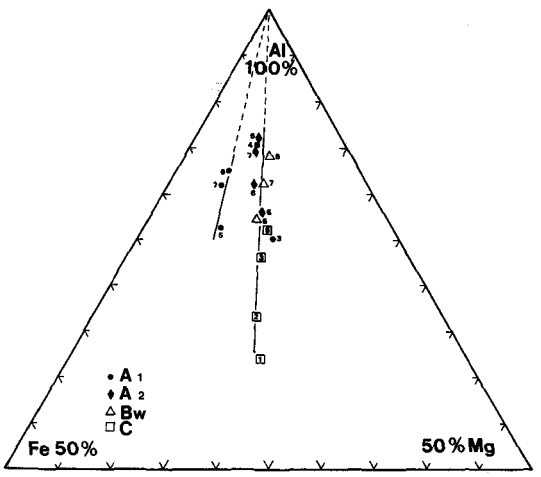

Figure 10. Relative contents in Al, Fe and Mg atoms in the separated fractions. 1: 10–20 μm; 2: 5–10 μm; 3: 2–5 μm; 4: 1–2 μm; 5: 0.2–1 μm; 6: 0.1–0.2 μm; 7: <0.1 μm.

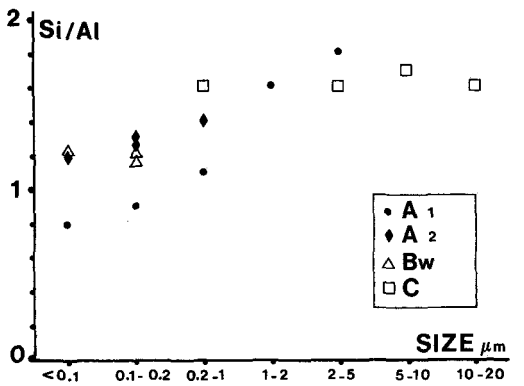

Figure 11. Si/Al atomic ratio for the separated fractions.

had totally disappeared from the coarse clay of that horizon (1–2 μm), but was found in the finer clay fraction (<1 μm). The same is true for the interstratified mica/vermiculite and vermiculite layers. These were present in the fine silt fractions but have disappeared from the A1 horizon coarse clays.

The distribution of mica layers in the different fractions was quite the opposite. Mica layers are the major component of the A1, 1–2 μm fractions, and their proportion progressively decreases with fraction size. Thus, it may be concluded that during fragmentation and/or simple transformation of the large phyllosilicates, clusters of chlorite, mica/vermiculite and vermiculite were preferentially affected. In good agreement is the decrease of the 0.153 and 0.154 nm XRD reflection intensities (trioctahedral minerals) and the increase of the 0.150 nm reflection (dioctahedral minerals) from the largest to the smallest particles. Ross (1975) and Vicente *et al.* (1977) have described changes during weathering from trioctahedral to dioctahedral structure. The peak at 0.153 nm could be attributed to an intermediate dioctahedral-trioctahedral structure and/or a strongly oxidized biotite (Fordham, 1990).

The relative decrease in the Mg and Fe atom contents could also be explained by preferential weathering of Fe,Mg-rich minerals (chlorite, trioctahedral vermiculite) from the coarse fractions. This resulted in the concentration of more resistant mica layers in the coarse clay fractions as the chlorite, mica/vermiculite and vermiculite residues were accumulated in the finer clays.

Table 5. Total analyses of selected fractions as percentage of dry sample.

Sample	SiO_2	Al_2O_3	Fe_2O_3	MnO	MgO	CaO	Na_2O	K_2O	TiO_2	Σ
A1										
2–5 M	52.20	22.60	5.59	0.09	2.32	0.20	1.26	4.67	1.79	90.72
1–2 M	50.69	26.10	4.06	0.08	1.67	0.27	1.45	4.80	1.49	90.61
0.2–1 M	35.59	27.62	8.67	0.14	1.93	0.12	0.94	4.51	2.02	81.54
0.1–0.2 T	32.66	30.07	6.77	0.09	1.54	0.04	0.69	4.31	1.51	77.68
<0.1 T	28.01	28.78	7.74	0.08	1.59	0.02	0.48	3.58	1.58	71.86
A2										
0.2–1 M	46.44	28.23	7.23	0.13	2.81	0.10	0.76	3.59	2.12	91.41
0.1–0.2 M	43.76	29.34	6.31	0.10	2.27	0.00	0.67	3.49	1.63	87.57
0.1–0.2 T	47.43	29.76	4.38	0.07	1.68	0.03	0.74	3.26	1.24	88.59
<0.1 T	41.91	28.22	4.74	0.06	1.71	0.00	0.60	2.63	1.34	81.21
Bw										
0.1–0.2 M	38.58	26.55	6.55	0.09	2.83	0.06	0.52	3.03	1.77	79.98
0.1–0.2 T	44.93	30.52	4.76	0.05	2.31	0.04	0.69	2.91	1.31	87.52
<0.1 T	41.72	28.97	6.67	0.05	2.50	0.01	0.66	2.40	1.25	84.23
C										
10–20 M	42.07	21.70	10.70	0.29	5.04	0.34	0.76	4.75	2.22	87.87
5–10 M	46.02	22.62	9.47	0.21	4.18	0.36	0.88	4.88	1.69	90.31
2–5 M	49.05	23.80	7.35	0.14	3.34	0.20	0.95	4.86	1.33	91.02
0.2–1 M	48.66	24.95	5.97	0.08	3.10	0.19	1.03	3.71	1.05	88.74

https://doi.org/10.1346/CCMN.1991.0390507 Published online by Cambridge University Press

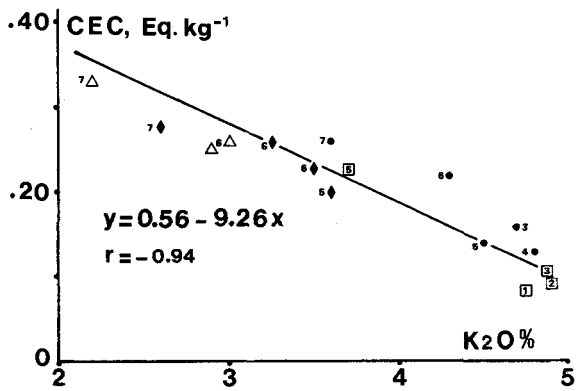

Figure 12. CEC vs nonexchangeable K_2O for the separated fractions. Symbols and figures as in Figure 10.

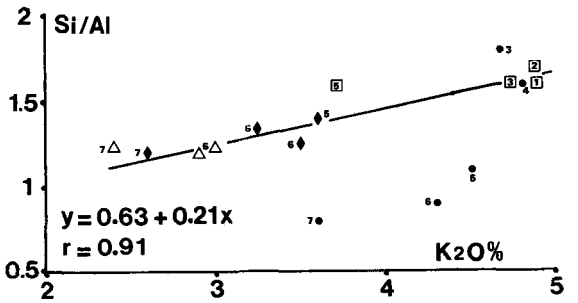

Figure 13. Si/Al atomic ratio vs nonexchangeable K_2O for the separated fractions. A1, 0.2–1, 0.1–0.2 and <0.1 μm samples are excluded from the correlation curve. Symbols and figures as in Figure 10.

Fe derived from the weathered minerals appears to accumulate in the finest fractions as amorphous and/or crystalline iron oxides. As these compounds were extracted by the CBD treatment, it was not possible to specify the type of iron oxides present. However, in acid brown soils developed from crystalline rocks, amorphous iron oxides generally account for the greatest part of the CBD-extractable Fe (Jeanroy *et al.*, 1984). The rather large amounts of material extracted by the CBD treatment indicate that, in addition to the transformation of phyllosilicates, dissolution was also an important weathering process in this soil.

If one makes the assumption that the finest fractions were also the most weathered, the changes from the 0.2–1 to the <0.1 μm T-fractions indicate that weathering proceeds through the transformation of mica layers to mica/vermiculite and vermiculite layers. Smectite layers were finally formed in the finest fraction. These minerals are dioctahedral. Smectite, vermiculite and interlayered mica/vermiculite were commonly described as weathering products of chlorite and/or mica in acid soils (Gjems, 1967; DeConinck and Herbillon, 1969; Bain, 1977; Ross *et al.*, 1982; Douglas, 1989).

A good agreement was found between the mineralogy of the various fractions, their K_2O content, and the CEC values. XRD showed a decrease of the proportion of mica layers from the larger to the finer fractions, while the proportions of interstratified vermiculite or smectite layers increased. This is consistent with a decrease in the K_2O content and an increase in the CEC.

Contrary to what might be expected, the K_2O content is higher in the A1, <0.1 μm T-fraction than in the equivalent Bw horizon sample that contained more mica layers. This might be explained if the A1 horizon mica layers did not occur as discrete particles, but were interstratified with the smectite and vermiculite layers.

The decrease of both the Si/Al atomic ratio and the K_2O content corroborates the relative accumulation of aluminum-rich minerals in the weathering products. Large proportions of kaolinite or gibbsite were not expected in the finest fractions, and XRD did not show increasing amounts of these minerals with a decrease in particle size. Moreover, increasing amounts of kaolinite and gibbsite would simultaneously lower both the CEC value and the K_2O content, and exactly the reverse was observed.

The composition of the three finest fractions from the A1 horizon showed higher Fe/Mg ratios than the others, suggesting that either the source minerals for these fine clays, or the weathering process were different. A clearly distinct behavior of these fractions was also observed on the Si/Al–K_2O diagram. For a given K_2O value the Si/Al ratios are lower than in the other samples. This indicates that the source minerals for the A1 horizon fine clays were not the same as for those of the Bw or A2 horizons. The lower Si/Al ratio could be explained by a higher proportion of weathered dioctahedral aluminous micas in these fractions. An increased hydroxy-Al interlayering could also be a reason for the decrease of the Si/Al ratio. However, subtraction of Al extracted by the Na-citrate treatment, and which was assumed to be interlayered hydroxy Al, did not significantly alter the Si/Al ratio. Moreover, an extended hydroxy-Al interlayering should have strongly reduced the CEC (Barnhisel and Bertsch, 1989). Such minerals should have a low CEC and a low K_2O content. As a consequence they would have diverged from the CEC–K_2O relationships.

HCl treatment has been used to dissolve chlorite and other weathered trioctahedral minerals (DeConinck *et al.*, 1975; Bain, 1977; Ross *et al.*, 1982). Adams and Kassim (1983) demonstrated that a 1 N HCl treatment virtually removed vermiculite produced from chlorite but had less effect on vermiculite produced from illite. Thus, the fact that about 90% of MgO (or K_2O) was extracted from the Bw, <0.1 μm T-fraction by the HCl treatment is indicative of a large proportion of chlorite and trioctahedral weathering products in this sample.

https://doi.org/10.1346/CCMN.1991.0390507 Published online by Cambridge University Press

Table 6. Composition of 1 N HCl extracts from A1 and Bw clay fractions.

Sample	Al_2O_3		Fe_2O_3		MgO		K_2O	
	(1)	(2)	(1)	(2)	(1)	(2)	(1)	(2)
A1 <0.1 μm T	167	59	71	92	7.5	47	17.7	49
Bw < 0.1 μm T	175	59	69	100	23.0	92	19.1	90

(1) g/kg, 105°C, dry sample; (2) percent total oxide.

Conversely, only about 50% of MgO (or K_2O) was extracted from the equivalent fraction from the A1 horizon. This suggests a higher chemical stability, attributed to a greater proportion of weathered dioctahedral phyllosilicates, for the A1 horizon fine clays.

Differences in the XRD behavior of the finest nonmagnetic fractions (<0.1 μm T-fraction) from either the Bw or the A1 horizons were also observed after Na-citrate treatment. Before treatment, the samples were typical of an intergrade vermiculite mineral (no expansion with ethylene glycol, incomplete collapse when K-saturated and heated). Following the Na-citrate treatment, the A1 horizon fraction exhibited an increased proportion of smectite layers and further collapse following K-saturation and heating. This is an indication that most of the interlayered material was extracted by the treatment. As the extract contains mainly Al and Fe, the hydroxy-Al and Fe interlayers are presumed to have been extracted. Although hydroxy-Fe compounds have been suggested (Singleton and Harward, 1971; Vicente-Hernandez *et al.*, 1983; Ghabru *et al.*, 1990), it is always possible that the Fe extracted by the Na-citrate treatment included some Fe-oxides incompletely removed by the previous CBD treatment, or Fe from the 2:1 layers themselves. The same would be true for a portion of the extracted Al.

Despite the fact that Fe and Al were extracted from the Bw horizon fraction at the same levels as from the A1 horizon fraction, only slight changes were observed in the XRD behavior of the treated Bw sample. A large part of the interlayered compounds was apparently not extracted. This could be the result of a more stable, better-organized hydroxy-Al (Fe) interlayered sheet. Such a hydroxy-Al (Fe) interlayered mineral should have a lower CEC than that of minerals in which interlayering is less pronounced (Barnhisel and Bertsch, 1989). This was not observed in the present instance. The CEC of the Bw-horizon fraction is greater than that of the A1 horizon. Thus, a more highly developed hydroxy-Al (Fe) interlayered sheet is not a satisfying explanation for the Bw horizon sample data.

Compared to the A1 fraction, far larger amounts of Mg were extracted from the Bw fraction by the Na-citrate treatment. This could be the result of partial dissolution of chlorite layers (Figure 7). Partial dissolution of chlorite with Na-citrate has been demonstrated by Ghabru *et al.* (1990). The poorly crystalline parts of the minerals were dissolved by the treatment which, however, did not result in the complete conversion of a true chlorite to vermiculite. Therefore, it is likely that a chlorite mineral with a more or less stable interlayer is a component of the Bw horizon fine clay fraction. As the Na-citrate treatment does not selectively dissolve the interlayered hydroxide sheet, the remaining undissolved minerals may contribute to the XRD intergrade behavior still observed for the treated sample.

The characteristics and origin of the finest nonmagnetic (T) fractions from either the A1 or the Bw horizons appear to be quite different. In the A1 horizon this fraction was identified mainly as a hydroxy-Al (Fe) intergrade smectite that may derived from the weathering of mica layers. In the Bw horizon the major component was an intergrade vermiculite originating, at least in part, from chlorite layers. These differences are likely to be linked to the A1 horizon being more acid and richer in organic matter than the Bw horizon. According to Schwertmann (1976), mafic chlorite is completely dissolved in strongly acid, organic soils, whereas it transforms to vermiculite in weakly acid, poorly organic soils.

The chemical analyses were plotted in the M^+-4Si-R^{2+} ternary system (Figure 14) but, as XRD showed that both coarse and fine fractions are composed of more than one phyllosilicate species, the chemical analysis represents the bulk composition of a mixture. This means that the linear trends depicted in Figure 14 must be interpreted as a two-component mixture. The extrapolation of a line was assumed to give the composition of one of the two pure components.

In Figure 14 the chemical analyses of the silt and coarse-clay fractions are distributed along a line joining the R^{2+}-pole on one side, and the composition of a high-charge beidellite on the other side. However, the high-charge beidellite pole is not reached and, moreover, beidellite was not identified by XRD in the coarse clays. Interpretation of Figure 14 corroborates the idea of preferential dissolution of vermiculite and chlorite layers, leaving a residue consisting of K-depleted, charge-reduced mica layers with Al in the octahedral sheet.

The chemical compositions of the fine clay fractions from the Bw and A2 horizons were clearly off of the coarse fraction line, indicating a change in weathering pathway. A decrease in layer charge and increase in Si-

https://doi.org/10.1346/CCMN.1991.0390507 Published online by Cambridge University Press

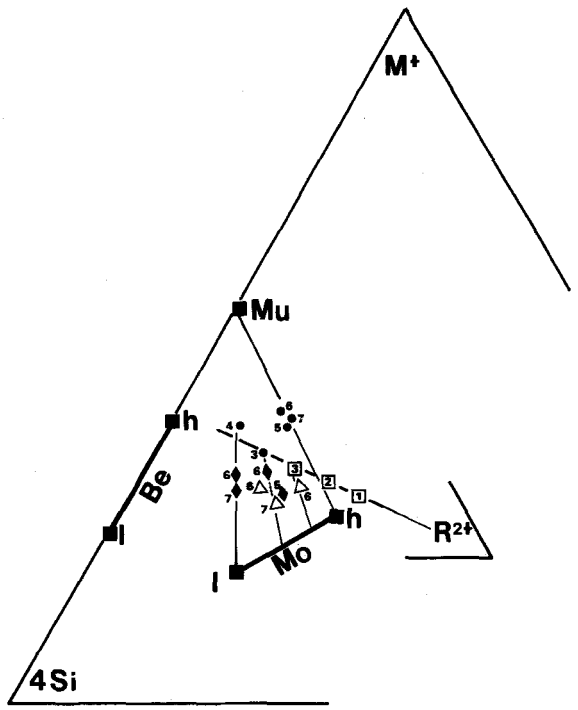

Figure 14. Chemical composition of the separated fractions in the M^+-4Si-R^{2+} ternary system. Mu: muscovite, Mo: montmorillonite, Be: beidellite, h: high charge, l: low charge. Symbols and figures as in Figure 10. Compositions of muscovite, beidellite and montmorillonite are from Meunier and Velde (1989).

atom content are involved. Although there is no direct evidence, such changes may indicate neoformation processes.

The chemical compositions are distributed along several lines joining montmorillonite in the M^+-4Si-R^{2+} diagram. Each transformed coarse mineral seemed to produce a montmorillonite. The weathering end products in the Bw and A2 horizons were not beidellite, as has been reported in other studies (Wilson, 1987). Buurman *et al.* (1976) have shown that smectites that had formed from chlorite in alpine soils were montmorillonite.

The composition of the fine clays from the A1 horizon are different from the others. They are on a line joining muscovite and high-charge montmorillonite. This represents a greater contribution of weathered dioctahedral micas in these fractions.

CONCLUSION

Size fractionation associated with HGMS has provided relatively homogeneous fractions of soil clays, greatly enhanced mineral characterization, and clarified possible weathering pathways. Weathering of large phyllosilicates preexisting in the saprolite involves physical fragmentation and mineralogical transformations. These processes vary according to the composition of the minerals and the physico-chemical characteristics of the soil horizons.

Chlorite and vermiculite are more strongly affected by physical fragmentation than the mica layers, contributing to the formation of the fine clays as mica residues accumulated in the coarse clay fractions. The most abundant end products of the weathering processes are hydroxy-Al(Fe) intergrade dioctahedral smectites in the A1 horizon and intergrade dioctahedral vermiculites in the less acid, less organic-rich Bw horizon. The intergrade character of vermiculite is related partly to hydroxy-Mg compounds.

The physical fragmentation of large particles is strongly related to chemical weathering. This process involves simultaneous loss of Fe and Mg from the mineral structure, leaving more aluminous dioctahedral minerals. Dissolution of the preexisting minerals leads to the precipitation of amorphous and/or crystalline Fe- and Al-oxides that are also important in the finest clays. Neoformation of phyllosilicate layers may not be excluded. The stable clay phase in this temperate, acid soil appears be a montmorillonite, the layer charge of which appears to be controlled by the composition of the precursor minerals.

REFERENCES

Adams, W. A. and Kassim, J. K. (1983) The origin of vermiculite developed from lower Palaeozoic sedimentary rocks in Mid Wales: *Soil Sci. Soc. Amer. J.* **47,** 316–320.

Bain, D. C. (1977) The weathering of chloritic minerals in some Scottish soils: *J. Soil Sci.* **28,** 144–164.

Barnhisel, R. I. and Bertsch, P. M. (1989) Chlorites and hydroxy interlayered vermiculite and smectite: in *Minerals in Soil Environments,* 2nd ed., J. B. Dixon and S. B. Weed, eds., Soil Sci. Soc. Amer., Madison, Wisconsin, 729–788.

Buurman, P., van der Plas, L., and Slager, S. (1976) A toposequence of alpine soils on calcareous mica schists, northern Adula region, Switzerland: *J. Soil Sci.* **27,** 395–410.

Churchman, G. J. (1980) Clay minerals formed from micas and chlorites in some New Zealand soils: *Clay Miner.* **15,** 59–76.

CPCS (1967) *Classification des sols:* ENSA, Thiverval-Grignon, 96 pp.

DeConinck, F., Conry, M., and Tavernier, R. (1975) Influence of iron-bearing minerals, especially chlorite, on soil development of Irish brown podzolic soils: *Proc. Int. Clay Conf.,* Applied Publishing, Wilmette, Illinois, 573–584.

DeConinck, F. and Herbillon, A. (1969) Evolution minéralogique et chimique des fractions argileuses dans des Alfisols et des Spodosols de la Campine (Belgique): *Pédologie* **XIX,** 159–272.

Douglas, L. A. (1967) Sodium citrate-dithionite induced alteration of biotite: *Soil Sci.* **103,** 191–195.

Douglas, L. A. (1989) Vermiculites: in *Minerals in Soil Environments,* 2nd ed., J. B. Dixon and S. B. Weed, eds., Soil Sci. Soc. Amer., Madison, Wisconsin, 635–674.

Fanning, D. S., Keramidas, V. Z., and El-Desoky, M. A. (1989) Micas: in *Minerals in Soil Environments,* 2nd ed., J. B. Dixon and S. B. Weed, eds., Soil Sci. Soc. Amer., Madison, Wisconsin, 551–634.

Fordham, A. W. (1990) Formation of trioctahedral illite

https://doi.org/10.1346/CCMN.1991.0390507 Published online by Cambridge University Press

from biotite in a soil profile over granite gneiss: *Clays & Clay Minerals* **38,** 187–195.

Ghabru, S. K., Mermut, A. R., and St. Arnaud, R. J. (1990) Isolation and characterization of an iron-rich chlorite-like mineral from soil clays: *Soil Sci. Soc. Amer. J.* **54,** 281–287.

Gjems, O. (1967) Studies on clay minerals and clay mineral formation in soil profiles in Scandinavia: *Med. Nor. Skogsgorsoeksues* **21,** 303–345.

Greene-Kelly, R. (1953) The identification of montmorillonoids in clays. *J. Soil Sci.* **4,** 233–237.

Jackson, M. L. (1963) Interlayering of expansible layer silicates in soils by chemical weathering: *Clays & Clay Minerals* **11,** 29–46.

Jeanroy, E. (1972) Analyse totale des silicates naturels par spectrophotométrie d'absorption atomique. Application au sol et à ses constituants: *Chim. Anal.* **54,** 159–166.

Jeanroy, E., Guillet, B., and Ortiz, R. (1984) Applications pédogénétiques de l'étude des formes du fer par les réactifs d'extraction: cas des sols brunifiés et podzolisés sur roches cristallines: *Science du Sol* **3,** 199–224.

Lanson, B. and Champion, O. (1991) The I/S to illite reaction in diagenesis: *Amer. J. Sci.,* (in press).

MacEwan, D. M. C. and Wilson, M. J. (1980) Interlayer and intercalation complexes of clay minerals: in *Crystal Structures of Clay Minerals and their X-ray Identification,* G. W. Brindley and G. Brown, eds., Mineralogical Society, London, 197–248.

Mehra, O. P. and Jackson, M. L. (1960) Iron oxide removal from soils and clays by a dithionite-citrate system buffered with sodium bicarbonate: *Clays & Clay Minerals,* **7,** 317–327.

Meunier, A. and Velde B. (1989) Solid solutions in I/S mixed layer minerals and illite: *Amer. Mineral.* **74,** 1106–1112.

Pédro, G. (1983) Structuring of some basic pedological processes: *Geoderma* **31,** 289–299.

Reynolds, R. C. (1980) Interstratified clay minerals: in *Crystal Structures of Clay Minerals and their X-ray Identification,* G. W. Brindley and G. Brown, eds., Mineralogical Society, London, 249–304.

Righi, D. and Borot, J. P. (1985) Présence de sols podzolisés à horizons Bh et Bs inversés sur le Plateau de Millevaches (Massif Central, France). *Science du Sol* **3,** 129–138.

Righi, D. and Jadault, P. (1988) Improving soil clay minerals studies by high-gradient magnetic separation: *Clay Miner.* **23,** 225–232.

Ross, G. J. (1975) Experimental alteration of chlorites into vermiculites by chemical oxidation: *Nature* **225,** 133–134.

Ross, G. J., Wang, C., Ozkan, A. I., and Rees, H. W. (1982) Weathering of chlorite and mica in a New Brunswick podzol developed on till derived from chlorite-mica schist: *Geoderma* **27,** 255–267.

Russell, J. D., Birnie, A., and Fraser, A. R. (1984) High-gradient magnetic separation (HGMS) in soil clay mineral studies: *Clay Miner.* **19,** 771–778.

Schwertmann, U. (1976) The weathering of mafic chlorites in soils (a review): *Z. Pflanzenern. Bodenk.* **1,** 27–36.

Singleton, P. C. and Harward, M. E. (1971) Iron hydroxy interlayers in soil clay: *Soil Sci. Soc. Am. Proc.* **35,** 838–842.

Stucki, J. W., Golden, D. C., and Roth, C. B. (1984) Effects of reduction and reoxidation of structural iron on the surface charge and dissolution of dioctahedral smectites. *Clays & Clay Minerals,* **32,** 350–356.

Tamura, T. (1958) Identification of clay minerals from acid soils: *J. Soil Sci.* **9,** 141–147.

USDA (1986) *Clés de la taxonomy des sols.* Monographie technique 13, Cornell University, Ithaca, New York, 347 pp.

Vicente, M. A., Razzaghe, M. H., and Robert, M. (1977) Formation of aluminium hydroxy vermiculite (intergrade) and smectite from mica under acidic conditions: *Clay Miner.* **12,** 101–112.

Vicente-Hernandez, J., Vicente, M. A., Robert, M., and Goodman, B. A. (1983) Evolution des biotites en fonction des conditions d'oxydo-réduction du milieu: *Clay Miner.* **18,** 267–275.

Weed, S. B. and Bowen, L. H. (1990) High-gradient magnetic concentration of chlorite and hydroxy-interlayered minerals in soils clays: *Soil Sci. Soc. Amer. J.* **54,** 274–280.

Wilson, M. J. (1987) Soil smectites and related interstratified minerals: Recent developments: in *Proc. Int. Clay Conf., Denver, 1985,* L. G. Schultz, H. van Olphen, and F. A. Mumpton, eds., The Clay Minerals Society, Bloomington, Indiana, 167–173.

(Received 29 November 1990; accepted 23 May 1991; Ms. 2056)

https://doi.org/10.1346/CCMN.1991.0390507 Published online by Cambridge University Press